scientific reports

Check for updates

OPEN

Unveiling the PEDOT-polypyrrole hybrid electrode for the electrochemical sensing of dopamine

Anandhavelu Sanmugam[1], C. Vanitha[2], Abdulrahman I. Almansour[3], K. Karuppasamy[4,5], T. Maiyalagan[6], Hyun-Seok Kim[7], Dhanasekaran Vikraman[7]✉ & Akram Alfantazi[4,5]✉

This study presents the electrochemical sensing of dopamine (DA) using an electrode of polypyrrole/poly(3,4-ethylenedioxythiophene) (PEDOT-PPy) thin film. Electrochemical analyses of the PEDOT-PPy thin film for DA sensing were conducted through cyclic voltammetry (CV) and differential pulse voltammetry (DPV). The CV analysis demonstrated that PEDOT-PPy exhibited superior electrochemical activity towards DA due to its enhanced conductivity as a high-conducting polymer composite. The DPV results indicated a linear concentration level of 5 nM to 200 µM with a minimal limit of sensing of 5 nM using the PEDOT-PPy electrode material. The fabricated sensor explored the sensitivity of 7.27 µA/µM cm^2 at the 5 to 1000 nM DA concentration and the dopamine diffusion coefficient of 1.3×10^{-8} cm^2/s. Additionally, the PEDOT-PPy electrode material displayed excellent reproducibility, selectivity, and stability. Therefore, the PEDOT-PPy composite electrode material shows excellent potential for outperforming other electrode materials in detecting DA.

Keywords PEDOT, Sensor, Polypyrrole, Dopamine, Electrochemical

The neurotransmitter dopamine (DA) shows an influential responsibility in maintaining the health of the hormonal, renal, cardiovascular, and central nervous systems in both vertebrates and invertebrates[1–3]. It is involved in regulating the body's sleep-wake cycle, movements, information flow, perception, motivation, stress responses, learning, cognitive skills, and memory. Abnormal DA levels can indicate various physiological illnesses, including neurodegenerative diseases like Parkinson's and Alzheimer's[1,4]. High levels of dopamine can cause hypertension, heart failure, and enlarged heart sweeps[5,6]. The construction of easy, responsive, and selective methodologies for the sensing of DA is needed to examine their range in the individual body[7,8]. There are various methods available to detect DA, including spectrophotometry, electrochemical, capillary electrophoresis, UV spectroscopy, and chemiluminescence techniques. However, some of the routes are experiencing difficulties due to the various species competing effects, exclusively ascorbic acid (AA) which owns an analogous oxidation potential[9,10]. Among these, electrochemical techniques have gained considerable benefits owing to their cheap and high response, sensitivity, and selectivity. Moreover, the development of nanomaterials has been established to be a proficient approach to DA detection. Recently, the application of nanomaterials with different arrangements of membranes, polymers, or biomolecules has been showing enhanced catalytic, sensing, and detection properties[11,12].

Experiments have shown that the enriched electrode characteristics are credited to the enhanced surface area and charge carriers[2,13]. Deposition of thick material strongly authorizes realizing the superior sensitivities, but it consumes a high response span owing to delayed adsorption and electron transferal processes[14]. The electrode surface topography influences cell adhesion, morphology, vascularity, protein adsorption, and activating the neural tissue[15]. The modifications of nano-porous structures on electrode surfaces have been exhibited to shrink

[1]Department of Applied Chemistry, Sri Venkateswara College of Engineering, Sriperumbudur 602117, India. [2]Department of Chemistry, Vel Tech Multi Tech Dr. Rangarajan Dr. Sakunthala Engineering College, Avadi, Tamilnadu, India. [3]Department of Chemistry, College of Science, King Saud University, P.O. Box 2455, Riyadh 11451, Saudi Arabia. [4]Department of Chemical and Petroleum Engineering, Khalifa University of Science and Technology, Abu Dhabi 127788, United Arab Emirates. [5]Emirates Nuclear Technology Center (ENTC), Khalifa University of Science and Technology, Abu Dhabi 127788, United Arab Emirates. [6]Department of Chemistry, SRM Institute of Science and Technology, Kattankulathur 603203, India. [7]Division of Electronics and Electrical Engineering, Dongguk University-Seoul, Seoul 04620, Republic of Korea. ✉email: v.j.dhanasekaran@gmail.com; akram.alfantazi@ku.ac.ae

the surroundings of the glial scar while sustaining neural cell union[16]. Conducting polymers are used to address limitations in preserving biological activity, biocompatibility, accessibility, and effective immobilization[14,17]. Polymers have many advantages over inorganic materials, such as the lack of toxicity, lower production costs, and greater availability of raw materials. High thermal conductivity is one of the barriers that prevent the improvement of the zero-turn of inorganic compounds[18]. Polymers have a one order of magnitude thermal conductivity which is lower than any semiconductor. One of the high frequently used conducting polymers of poly(3,4-ethylenedioxythiophene) (PEDOT) has shown strong consideration owing to its tremendous electrochemical and optical characteristics[19,20]. PEDOT is easily obtained through the anodic oxidation of the appropriate monomer, surprisingly in an aqueous bath, with numerous anionic counter-ions[21]. Composite polymer PEDOT: Nafion embedded with carbon fiber resulted in the improved sensitivity associated with pure-form electrode outcomes along with a small 4–5 nM DA limit of detection (LOD)[22]. Electrochemically copolymerized PEDOT interconnected graphene oxide on a carbon fibre sensor attained an enormous increment in DA sensing and a half decrement in LOD on the implanted rat's dorsal striatum compared to bare electrodes[23]. Oxidative etched carbon nanofibres resulted in the enhancement of surface oxide ensembles for DA adsorption and the interference AA species repulsion with a low LOD of 6 nM[24].

In functional hybrid networks, cells can attach adhesion molecules owing to the rough and porous surfaces, which improves sensor integration into neural tissue. By tuning the nanofibers on the geometry of the surface, it is possible to manage the centralized reaction in neural tissue. In recent times, nanostructured polypyrrole (PPy) based sensing has been a hot topic to involve significant research due to its potential high conductivity, firmness, and adaptability for employing various kinds of applications[25,26]. PPy has been extensively studied because of its many specific properties for electrochemical sensing, electrochemical energy storage, etc., which have clear benefits over bulk structure[27]. Usually, PPy can be prepared by chemically and electrochemically oxidizing the monomer under mild conditions. Typically, electrochemically coated PPy composite films are highly conductive but have low optical transparency. These composite polymers offer significant advantages over single-conductive polymers in terms of chemical and mechanical behaviors. Additionally, conducting polymer blends have several fascinating properties associated with other typical inorganic composites. The conductive polymer composites have a very low-level separation parameter in their conductivity concerning the fabrication procedure. In addition, polymer-polymer blends create steady modification on the separation threshold which enhances the resulting composites' electrical conductivity. For instance, Zhao et al.[28] have deliberately elaborated electrochemical patch wearable sensors for instantaneous DA and glucose detection in sweat. In addition, Delmo et al. have summarized the most current developments in in vivo DA detection using various kinds of sensing materials[29].

Herein, we report the polymerization of the PEDOT-PPy hybrid structure onto the glassy carbon electrode (GCE) for effective electrochemical DA determination. The cyclic voltammetry (CV) analysis demonstrated that PEDOT-PPy exhibited superior electrochemical activity towards DA due to its enhanced conductivity as a high-conducting polymer composite. The observed results revealed high selectivity and sensitivity of the assembled electrochemical DA sensor.

Results and discussion

Figure 1a–c shows the morphological image of PEDOT, PPy and PEDOT-PPy composite. The rough surface of PEDOT was observed as shown in Fig. 1a which paved the way for easy formulation of composites. In the case of PPy (Fig. 1b), SEM image explores the agglomerated surface composed of spherical and patchy grains with porous nature. PEDOT-PPy produced the coarse morphology as shown in Fig. 1c. The surface produces the hillocks and inhomogeneous grains due to composite formulation. The observed open structure of PEDOT-PPy leads to a large surface area for better sensory application. Figure 1d-f shows the FTIR profiles of PEDOT, PPy and PEDOT-PPy electrodes, respectively. The observed profiles of PEDOT explore the peak at 1523 and 1485 cm^{-1} relates to the C = C and C-C stretching mode, respectively[30]. In addition, the peaks are at 1296 cm^{-1} assigned to the –C-O-C stretching vibration. The = C–H out-of-plane and in-plane vibrations are observed at 1116 and 996 cm^{-1}, respectively[31]. C–S–C bonding vibration is observed at 682 and 814 cm^{-1} for PEDOT. The FTIR spectrum appears the principal characteristic peak at ~ 822 and 921 cm^{-1} relating to characteristic PPy structure[32]. The = C–H in-plane and deformation vibrations peaks of PPy are observed at 1122 and 1062 cm^{-1}, respectively[33,34]. N–H deformation peak observed at 1376 cm^{-1} from the PPy structure[35]. The C–N and C = C bending vibrations are observed at 1592 and 1637 cm^{-1}, respectively. Peaks from PEDOT-PPy about 680 and 810 cm^{-1} undeniably signify the C–S–C and PPy structure, respectively which is credited to the composite formation[36]. The typical C–H in-plane peak indisputably appears at around 1118 cm^{-1}. C–S–C, C–C and C=C peaks are observed for the composites[37].

The CVs were performed under 1 mM $[Fe(CN)_6]^{3-/4-}$ in 0.1 M of KCl at a scan rate of 50 mV/s. Figure 2a shows the CVs of bare GCE and PPy, PEDOT, and PEDOT-PPy modified GCE electrodes. The observed CV for the bare electrode is well correlated with the literature[38,39]. However, modified electrodes using PEDOT and PPy on the GCE, and CV profiles indicate the strong peak current for the reduction of $[Fe(CN)_6]^{3-/4-}$ at 2.9 mA and 3.6 mA, respectively. However, the altered PEDOT-PPy/GCE electrode has drastically increased the reduction peak current to 4.6 mA among the different prepared electrodes. This behavior is attributed to the increased conductivity of composite electrode surface by the enhanced electroactive surface area and hybrid polymers. The modified electrode conductivity studies were done by EIS, which gives valuable details due to the different polymer infusion characteristics. The carrier transport kinetics of the PPy, PEDOT, and PEDOT-PPy electrodes were monitored by EIS profile at the electrode/electrolyte interface. The semicircle portion of the curve represents the electron-transmission rationing behavior. Figure 2b demonstrates the impedance profiles of bare and PPy, PEDOT, and PEDOT-PPy modified GCE electrodes at 25 mV polarization voltage and 1 Hz–1 MHz frequency range. The Nyquist graphs reveal the R_s values of 85, 70, 63, and 44 Ω for the bare and PPy, PEDOT, and PEDOT-

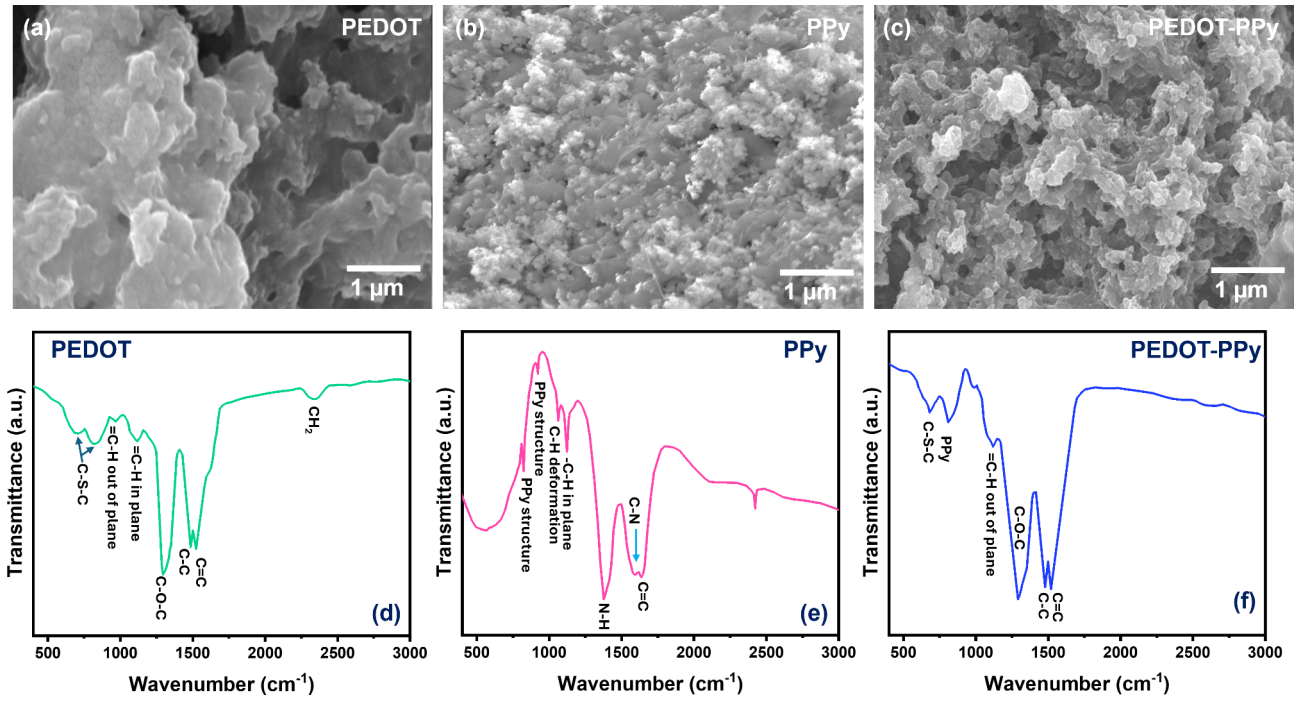

Fig. 1. Scanning electron microscopic image of (**a**) PEDOT, (**b**) PPy and (**c**) PEDOT-PPy; FTIR profiles of (**d**) PEDOT, (**e**) PPy and (**f**) PEDOT-PPy.

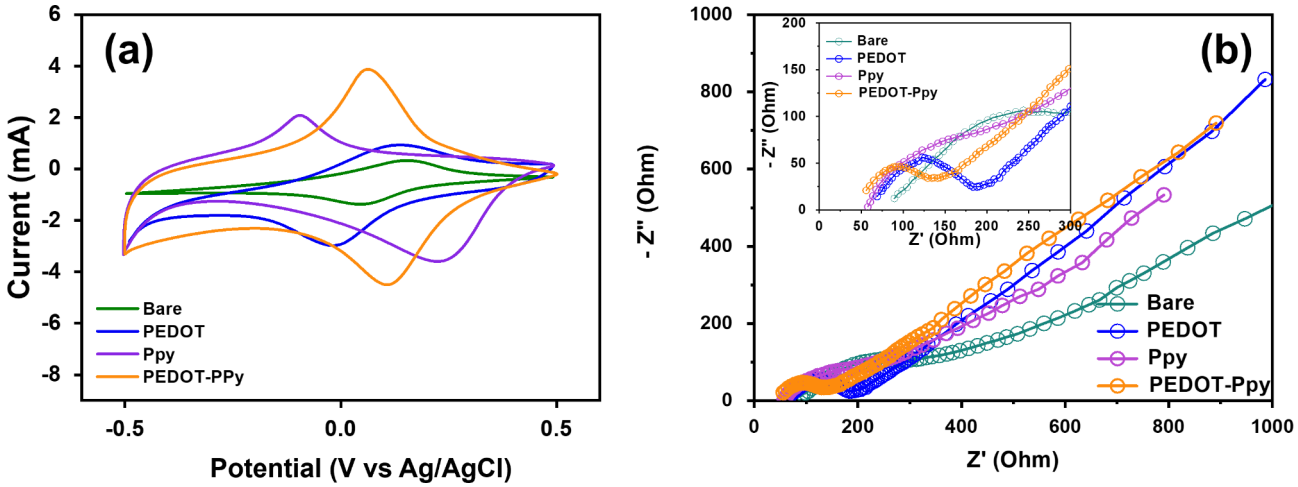

Fig. 2. (**a**) Cyclic voltammetry and (**b**) EIS spectra (inset-zoomed part) with the presence of ferri/ferrocyanide in 0.1 M of KCl for bare GCE, PEDOT, PPy, and PEDOT-PPy.

PPy modified GCE electrodes, respectively. The charge-transference resistance of PEDOT-PPy-GCE is small compared to other prepared electrodes. With the polymer composites modified electrode, the diminished R_{ct} outcome realized at 230, 135, 112, and 68 Ω for the bare and PPy, PEDOT, and PEDOT-PPy modified GCE electrodes, respectively which implies the enhanced conductive behavior. The electrochemically active surface area (ECSA) for PEDOT-PPy modified GCE electrode was estimated by engaging the CV at different scan speeds in 1 mM $[Fe(CN)_6]^{3-/4-}$ in 0.1 M of KCl[40]. Figure S1a shows the CV of PEDOT-PPy modified GCE electrode at different scan speeds. The C_{dl} was derived from the line fitting of current differences (i_d) between the cathodic and anodic peaks at -0.05 V vs. Ag/AgCl[41,42]. Figure S1b shows the fitted line profiles for the PEDOT-PPy, PPy and PEDOT modified GCEs. The estimated C_{dl} values are at 8.38, 5.01 and 4.25 µF/cm^2 for PEDOT-PPy, PPy and PEDOT, respectively. The estimated ECSA values are 0.21, 0.12 and 0.10 cm^2 for PEDOT-PPy, PPy and PEDOT, respectively. Thus, enhanced sensing activity of the PEDOT-PPy composites compared to their pure form is produced by enhanced intrinsic activity of composite active facets rather than the high number of active edges. The peculiarities of the electrochemical modified process of GCE with PEDOT-PPy increase the conductance

towards the electrochemical oxidation of $[Fe(CN)_6]^{3-/4-}$[43]. These outcomes exhibit that the conducting surface has increased on PEDOT-PPy-GCE. This can lead the high conducting kinetic paths between the electrolyte/electrode interrelations and gives a proficient stage for sensing uses. The initial results acquired propose that the modified GCE could act as efficient electrodes for DA detection.

To realize the DA detection, CV experiments were performed for the prepared electrodes in 0.1 M PBS buffer (pH 7) solution with the presence of 50 µM DA at pH 7.0. Figure 3a shows a CV profile at 50 mV/s scan rate of the pure GCE, PPy-GCE, PEDOT-GCE, and PEDOT-PPy-GCE. The results explore the reversible peak with strong current responses for the polymer-modified electrodes. The rise in the redox current values for the PPy-GCE, PEDOT-GCE, and PEDOT-PPy-GCE signified the catalyzing effect of electrodes for the DA oxidation and the depletion of the o-dopaquinone which materialized in oxidation[44]. The observed results reveal the maximum current response for DA detection by the PEDOT-PPy-GCE electrode. High peak current observation for DA by PEDOT-PPy-GCE than the PPy-GCE and PEDOT-GCE endorsed the increased catalytic activity, conductivity, and electroactive surface area. Incorporation of PEDOT in the matrix of PPy has resulted in enriched synergistic behavior and interacted ions transportation realizes the improved detection of DA[45].

The influence of potential scan rate for DA detection using 50 µM with pH 7.0 was examined by CV for the high-rate sensor of PEDOT-PPy-GCE. The result shows an increment in the reduction and oxidation currents with the enrichment of the scan rate from 10 to 150 mV/s (Fig. 3b). The shift of oxidative cathodic peak towards the positive and anodic peak towards the negative potential of DA as the scan rate enhanced which implies the DA reversible electrochemical reduction/oxidation[46]. The relation between the peak current (cathodic and anodic) in terms of the square root of the scan rate exposed diffusion influenced redox reactions. The anodic and cathodic peak currents of DA ($I_{p.a.}$ and I_{pc}) detection were continually enriched with scan rates square roots

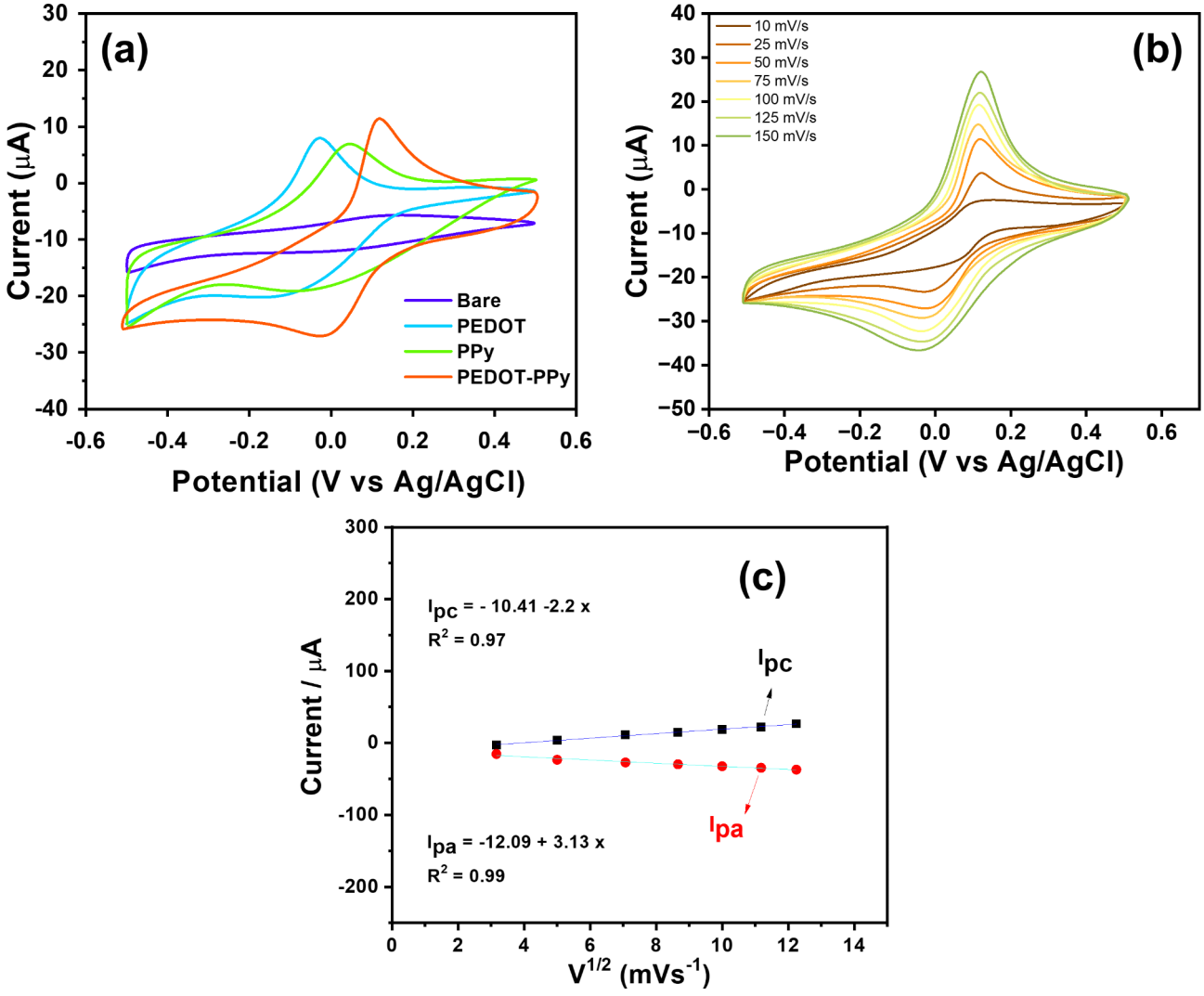

Fig. 3. (**a**) CVs of the bare, GCE, PEDOT, PPy, and PEDOT-PPy under 50 µM of DA in pH 7.0 PBS solution at 50 mV/s; (**b**) scan rate profiles (10–150 mV/s) for PEDOT-PPy sensor under 50 µM of DA in pH 7.0 PBS solution and (**c**) their correlation graph of inverse scan rate vs. current.

as shown in Fig. 3c, which implied the diffusion-presided detection process. The following linear regression relations are linked to the reduction and oxidation of DA detection kinetics,

Anodic:

$$I_{pa}\,(\mu A) \;=\; -12.09 + 3.13x\; v^{1/2},\; with\; R^2 = 0.99 \tag{1}$$

Cathodic:

$$I_{pc}\,(\mu A) \;=\; -10.41 - 2.2x\; v^{1/2} with\; R^2 = \;0.97 \tag{2}$$

Moreover, by Randles-Sevcik equation was used to estimate the diffusion coefficient of the prepared sensor[47]. The calculated diffusion coefficient of the assembled PEDOT-PPy-GCE sensor is 1.3×10^{-8} cm^2/s.

pH is a significant parameter to set the amperometric behavior of the detection of DA. Initially, 50 µM DA analyte was prepared in different pH solutions (pH = 4–9). Differential pulse voltammetry (DPV) experiments were carried out for the prepared DA analyte under identical experimental conditions. In each study, the peak current was measured, and it was correlated with different pH. Figure 4a displays the DPV profiles obtained encompassing 50 µM DA in PBS solution with pH of 4.0, 5.0, 6.0, 7.0, 8.0 and 9.0. The influence of pH on the retort current of the PEDOT-PPy sensor was exposed through the correlation graph (Fig. 4b). The standard deviation from the replicated measurement is given in the Fig. 4b. From the observed results, the current value enhanced from 4.0 to 7.0 which is related to the enriching dissociation characteristics of surface-involved acid groups as pH surges, synchronizing the enrichment of electrostatic attraction signal among the surface of the electrode and DA. The peak current diminishes further increasing pH owing to the loss of DA protons, thereby developing the neutral species[46]. The maximum current response was observed for DA detection with pH 7.0 for the PEDOT-PPy sensor electrode. Thus, the optimum pH for DA detection is fixed as pH 7.0.

To estimate the concentration range of DA, a DPV calibration profile was engaged for the PEDOT-PPy-GCE electrode. Figure 5a shows the DPV voltammograms of DA with different known concentrations from 5 nM -200µM under identical experimental conditions for the PEDOT-PPy-GCE electrode. The obtained voltammograms' oxidation peak current was noted to identify the role of DA concentrations. The peak currents were correlated with the DA concentration[48]. The concentration of DA is found to be directly proportional to the response current (Fig. 5b). The catalytic reaction shows a first-order reaction for the linear range of increments. The linear level of DA concentrations explores a sensing level of 5 nM to 200 µM. The obtained LOD is to be 5 nM at S/*N* = 3 (signal-to-noise ratio) which is comparable to the various literature outcomes including enzyme-based carbon fiber and tyrosinase-based biosensor[49,50]. The sensitivities of PEDOT-PPy-GCE in the lower concentration range (5–1000 nM) and higher concentration range (10–200 µM) are at 7.27 µA/µM cm^2 and 0.36 mA/µM cm^2, respectively. The experimental outcomes exposed that the prepared PEDOT-PPy electrode produces swift and high-accuracy DA detection. An outline of DA concentration and inverse current was employed to obtain the highest current response (I*max*). The obtained high I*max* indicates the capability of prepared electrode material for the sensing of DA at low and high concentrations[51].

An interference study was carried out for the PEDOT-PPy electrode. Figure 6a shows the DPVs of the PEDOT-PPy electrode sensor with the different interfering molecules such as glucose, uric acid, ascorbic acid, ethylamine, and gallic acid in 0.1 M PBS solution. The amount of interfering molecules was used 10 times associated with the dopamine concentration (50 µM). The observed redox reaction indicates the selective detection of the prepared PEDOT-PPy electrode sensor[52]. Further, the current profile indicates the selective detection of prepared PEDOT-PPy electrodes among the various interfering agents such as glucose, uric acid,

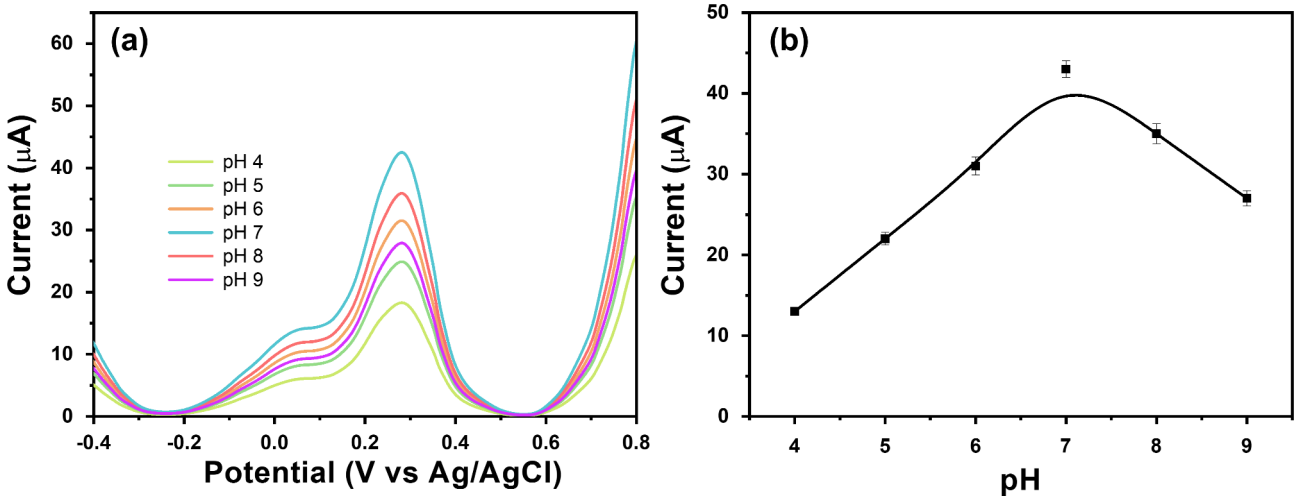

Fig. 4. (**a**) Differential pulse voltammetry at the various pH and their (**b**) correlation profile of current vs. pH for PEDOT-PPy sensor (error bar defines the standard deviation from the replicated measurement).

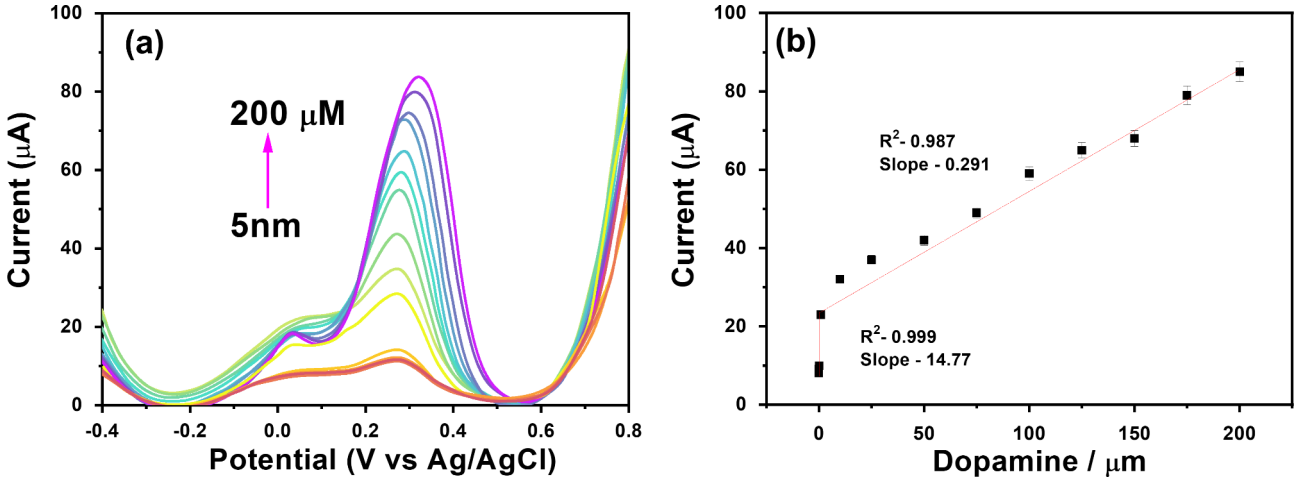

Fig. 5. (**a**) Differential pulse voltammetry for the different DA concentrations from 5 nM to 200 µM of PEDOT-PPy; (**b**) Correlation graph of concentration of DA vs. current ($n = 3$).

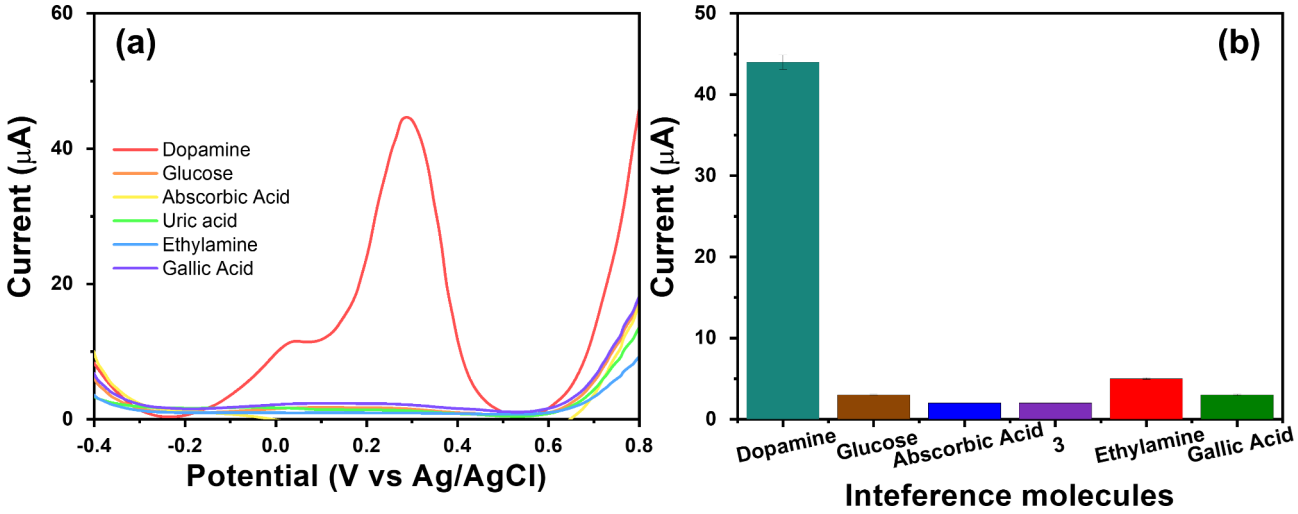

Fig. 6. (**a**) DPV profile of PEDOT-PPy sensor with the different interference molecules; (**b**) Current profile under the presence of various biomolecules for PEDOT-PPy.

ascorbic acid, ethylamine, and gallic acid were studied using differential pulse voltammetry. Figure 6b shows the DPV profile current response of dopamine, glucose, uric acid, ascorbic acid, ethylamine, and gallic acid. There is no significant change in the electrode response towards the DA sensor. The observed results strongly established the selective sensitivity of prepared PEDOT-PPy sensors toward dopamine detection. Table S1 summarizes the comparison of various sensor outcomes with PEDOT-PPy-GCE. Zhong et al.[53] have observed linearity of 0.05-10 µM and detection limit of 0.033 µM for the pyrrole-phenylboronic acid electrode. The detection limit of 1 nm and sensitivity of 6.33 µA/µM were observed for the PPy-RGO electrode[54].

Figure 7a shows the DPV profile of the PEDOT-PPy sensor for the continuous 50 cycles. The observed results further revealed the stout durability of dopamine detection[55]. Furthermore, the key feature of reproducibility behavior was examined by determining the electrode DPV profiles in buffer pH 7.0 PBS solution with 150 µM DA every 5 days. The sensor device was kept at 4 °C in the dark and exposed to reproducibility studies every 5 days. Figure 7b shows the reproducibility of the electrode which explores the minimal decrement of the response current at the initial level. The gradual decrement observed in the response is current after 30 days and keeps about 89% of its primary response after 60 days. Thus, the modified electrode shows good stability and good reproducibility towards DA determination. The detection with the PEDOT-PPy composite was experimented with sense DA in serum samples. Before the experiment, the 50 times dilution of real samples was done with PBS (pH 7.0)[56]. Table S2 compares the outcomes of different amounts of DA in blood samples. The recovery ranged from 106 to 120% with a standard deviation (RSD, $n = 3$) of less than 5%. These outcomes suggested that the flexible sensor with the PEDOT-PPy composite is appropriate for low-level DA sensing applications.

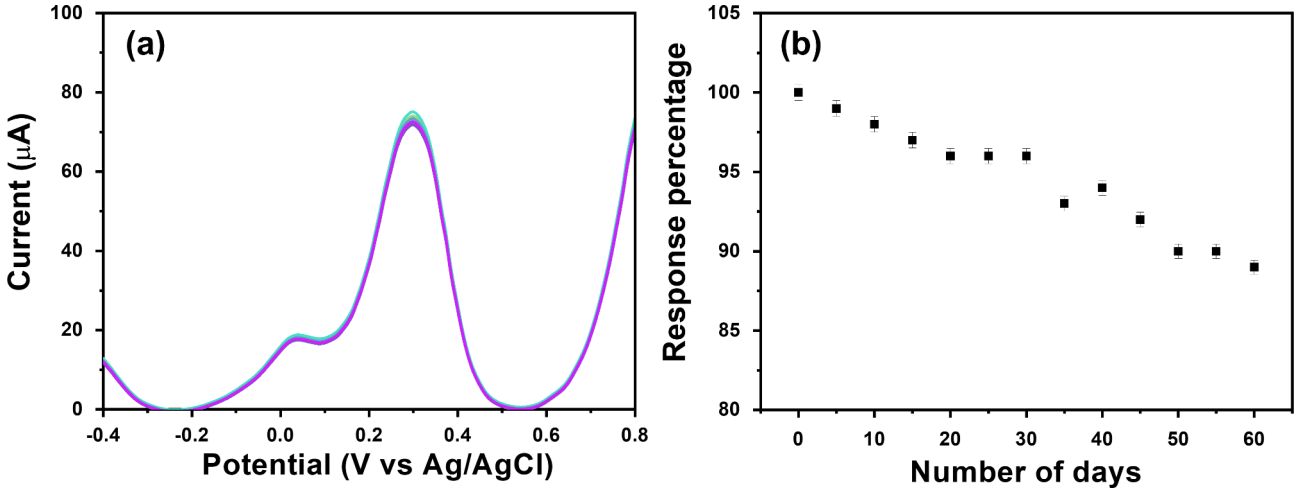

Fig. 7. (**a**) DPV stability profiles of PEDOT-PPy electrode for DA detection with 150μM of DA and (**b**) Response percentage of PEDOT-PPy sensor for the 60 days ($n = 3$).

Conclusions

A facile route was employed to fabricate the PEDOT-PPy sensor electrode on the GCE through an electrochemical polymerization process. FTIR and SEM studies explored the functional and surface properties of prepared sensor electrodes, respectively. Cyclic voltammetric studies explored the extensive detection of prepared electrodes for DA. In addition, the pH sensitivity was systematically analyzed for a better range of DA detection. DPV studies revealed the correlation between restart current and concentration of DA. The realized linear level of DA concentration was 5 nM to 200 μM and the LOD was 5 nM at $S/N = 3$. The sensitivity of the fabricated sensor was at 7.27 μA/μM cm^2 for the 5 to 1000 nM DA concentration. The dopamine diffusion coefficient approximation at the polymer composite surface was over the range of 1.3×10^{-8} cm^2/s. The selectivity and sensitivity among the various interference materials on the DA proved the compatibility of the PEDOT-PPy sensor. The duplicability and solidity of the sensor electrode strongly authorized the capability of PEDOT-PPy for a better range of DA detection. The real sample analysis of the fabricated PEDOT-PPy composite sensor confirmed the feasibility of DA sensing.

Experimental details

A polymerization process was employed to form the PEDOT-PPy hybrid structured on the glassy carbon substrate. A conventional three-electrode electrochemical unit (CHI760) was employed for the PEDOT-PPy formation at room temperature. The PEDOT-PPy film was coated by electro-polymerization procedure on the GCE using an electrolyte encompassing 10 mM of PEDOT and 10 mM of PPy. Initially, voltammograms from − 0.4 to 0.8 V vs. Ag/AgCl at 50 mV/s scan rate were performed for the sample stability. Then, electrochemical reduction of PEDOT-PPy was done by potentiostatic mode with the pH 7.4 solution for 600s by utilizing − 0.9 V[57]. Fourier transform infrared (FTIR) spectral results were procured from the PerkinElmer Spectrum 400 spectrometer. The surface morphological results were obtained using a scanning electron microscope (SEM), JEOL JSM-7600 F. Electrochemical analytical studies such as CV, DPV, and electrochemical impedance spectroscopy (EIS) were recorded by a CHI760 (USA) workstation. All electrochemical studies were done using the prepared working electrode on GCE along with the Ag/AgCl and platinum wire as the reference and counter electrode, respectively.

Data availability

The datasets used and/or analysed during the current study available from the corresponding author on reasonable request.

Received: 15 July 2024; Accepted: 4 December 2024
Published online: 31 March 2025

References

1. Grill, F. et al. Dopamine release in human associative striatum during reversal learning. *Nat. Commun.* **15**, 59 (2024).
2. Robinson, D. L., Hermans, A., Seipel, A. T. & Wightman, R. M. Monitoring rapid chemical communication in the brain. *Chem. Rev.* **108**, 2554–2584 (2008).
3. Ahmed, J., Faisal, M., Algethami, J. S., Alsaiari, M. & Harraz, F. A. A novel In2O3-doped ZnO decorated mesoporous carbon nanocomposite as a sensitive and selective dopamine electrochemical sensor. *J. Mater. Res. Technol.* **29**, 540–549 (2024).
4. Medina-Luque, J., Piechocinski, P., Feyen, P., Sgobio, C. & Herms, J. Striatal dopamine neurotransmission is altered in age- and region-specific manner in a Parkinson's disease transgenic mouse. *Sci. Rep.* **14**, 164 (2024).
5. Wilson, G. S. & Gifford, R. Biosensors for real-time in vivo measurements. *Biosens. Bioelectron.* **20**, 2388–2403 (2005).

6. Klein, M. O. et al. Dopamine: functions, signaling, and association with neurological diseases. *Cell. Mol. Neurobiol.* **39**, 31–59 (2019).
7. Shashikumara, J. K., Swamy, B. E. K., Sharma, S. C., Hariprasad, S. A. & Mohanty, K. Poly (red DSBR)/Al-ZnO modified carbon paste electrode sensor for dopamine: a voltammetric study. *Sci. Rep.* **11**, 14310 (2021).
8. Shashikumara, J. K. et al. Effect of RGO-Y2O3 and RGO-Y2O3:Cr3 + nanocomposite sensor for dopamine. *Sci. Rep.* **11**, 9372 (2021).
9. Anuar, N. S., Basirun, W. J., Shalauddin, M. & Akhter, S. A dopamine electrochemical sensor based on a platinum–silver graphene nanocomposite modified electrode. *RSC Adv.* **10**, 17336–17344 (2020).
10. Hussain, S. & Zaidi, S. A. Facile preparation of molybdenum carbide (Mo_2C) nanoparticles and its effective utilization in electrochemical sensing of folic acid via imprinting. *Biosens. Bioelectron.* **140**, 111330 (2019). Vikraman, D.Kim, H.-S. & Jung, J.
11. Pingarrón, J. M. & Yáñez-Sedeño, P., González-Cortés, A. Gold nanoparticle-based electrochemical biosensors. *Electrochim. Acta*. **53**, 5848–5866 (2008).
12. Muñoz, F. F. et al. Novel ce(OH)CO_3/carbon nanotubes hybrid material towards a highly sensitive electrochemical dopamine determination in real urine samples. *Electrochim. Acta*. **488**, 144194 (2024).
13. Guo, H. et al. Imine-linked covalent organic framework with high crystallinity for constructing sensitive purine bases electrochemical sensor. *J. Colloid Interface Sci.* **659**, 639–649 (2024).
14. Chen, J., Ding, X. & Zhang, D. Challenges and strategies faced in the electrochemical biosensing analysis of neurochemicals in vivo: a review. *Talanta* **266**, 124933 (2024).
15. Liang, H. et al. Carbon fiber microelectrode array loaded with the diazonium salt-single-walled carbon nanotubes composites for the simultaneous monitoring of dopamine and serotonin in vivo. *Anal. Chim. Acta* **1186**, 339086, (2021).
16. Martinez, J. G., Mehraeen, S. & Jager, E. W. H. Electrochemical considerations for the electropolymerization of PPy on PEDOT:PSS for yarn actuator applications. *ChemElectroChem* **10**, e202300188 (2023).
17. Kanwal, R. et al. Polypyrrole coated carbon fiber/ magnetite/ graphene oxide reinforced hybrid epoxy composites for high strength and electromagnetic interference shielding. *Mater. Today Commun.* **38**, 107684 (2024).
18. Zhang, X., Zhang, B., Ouyang, X., Chen, L. & Wu, H. Polymer solar cells employing water-soluble polypyrrole nanoparticles as dopants of PEDOT:PSS with enhanced efficiency and stability. *J. Phys. Chem. C.* **121**, 18378–18384 (2017).
19. Culebras, M., Uriol, B., Gómez, C. M. & Cantarero, A. Controlling the thermoelectric properties of polymers: application to PEDOT and polypyrrole. *Phys. Chem. Chem. Phys.* **17**, 15140–15145 (2015).
20. Ren, X. et al. Highly conductive PPy–PEDOT:PSS hybrid hydrogel with superior biocompatibility for bioelectronics application. *ACS Appl. Mater. Interfaces*. **13**, 25374–25382 (2021).
21. Luo, X., Weaver, C. L., Tan, S. & Cui, X. T. Pure graphene oxide doped conducting polymer nanocomposite for bio-interfacing. *J. Mater. Chem. B*. **1**, 1340–1348 (2013).
22. Vreeland, R. F. et al. Biocompatible PEDOT:Nafion composite electrode coatings for selective detection of neurotransmitters in vivo. *Anal. Chem.* **87**, 2600–2607 (2015).
23. Taylor, I. M. et al. Enhanced dopamine detection sensitivity by PEDOT/graphene oxide coating on in vivo carbon fiber electrodes. *Biosens. Bioelectron.* **89**, 400–410 (2017).
24. Puthongkham, P., Yang, C. & Venton, B. J. Carbon nanohorn-modified carbon fiber microelectrodes for dopamine detection. *Electroanalysis* **30**, 1073–1081 (2018).
25. Li, Y., Jiang, C. & Han, W. Extending the pressure sensing range of porous polypyrrole with multiscale microstructures. *Nanoscale* **12**, 2081–2088 (2020).
26. Tighilt, F. Z. et al. Mesoporous silicon/polypyrrole based structures for paranitrophenol sensing. *Silicon* **14**, 4149–4155 (2022).
27. Hao, L., Dong, C., Zhang, L., Zhu, K. & Yu, D. Polypyrrole nanomaterials: structure, preparation and application. *Polymers* **14**, 5139 (2022).
28. Zhao, J., Guo, H., Li, J., Bandodkar, A. J. & Rogers, J. A. Body-interfaced chemical sensors for noninvasive monitoring and analysis of Biofluids. *Trends Chem.* **1**, 559–571 (2019).
29. Delmo, N., Mostafiz, B., Ross, A. E., Suni, J. & Peltola, E. Developing an electrochemical sensor for the in vivo measurements of dopamine. *Sens. Diagn*. **2**, 559–581 (2023).
30. Ly, C. T. et al. Electrodeposition of PEDOT-rGO film in aqueous solution for detection of acetaminophen in traditional medicaments*. *Adv. Nat. Sci. NanoSci. NanoTechnol.* **10**, 015013 (2019).
31. Devaki, S. J., Sadanandhan, N. K., Sasi, R., Adler, H. J. P. & Pich, A. Water dispersible electrically conductive poly(3,4-ethylenedioxythiophene) nanospindles by liquid crystalline template assisted polymerization. *J. Mater. Chem. C.* **2**, 6991–7000 (2014).
32. Kulandaivalu, S. & Sulaiman, Y. Rational design of layer-by-layer assembled polypyrrole-based nanocomposite film for high-performance supercapacitor. *J. Mater. Sci. Mater. Electron.* **31**, 4882–4894 (2020).
33. Navale, S. T. et al. Highly selective and sensitive room temperature NO2 gas sensor based on polypyrrole thin films. *Synth. Met.* **189**, 94–99 (2014).
34. Jeon, S. S., Park, J. K., Yoon, C. S. & Im, S. S. Organic single-crystal surface-induced polymerization of conducting polypyrroles. *Langmuir* **25**, 11420–11424 (2009).
35. Maruthamuthu, S. et al. CuBr-induced charge screening on photoactive nanocolloidal polypyrrole:poly(styrene sulfonate) composite multilayer thin-film counter electrodes for high-efficiency dye-sensitized solar cells. *Polym. Int.* **65**, 584–595 (2016).
36. Kharat, H. J. et al. Synthesis of polypyrrole films for the development of ammonia sensor. *Polym. Adv. Technol.* **18**, 397–402 (2007).
37. Brijesh, K., Bindu, K., Shanbhag, D. & Nagaraja, H. S. Chemically prepared polypyrrole/ZnWO4 nanocomposite electrodes for electrocatalytic water splitting. *Int. J. Hydrog. Energy*. **44**, 757–767 (2019).
38. Zhang, Y. et al. Amperometric hydrogen peroxide sensor using a glassy carbon electrode modified with a nanocomposite prepared from ferumoxytol and reduced graphene oxide decorated with platinum nanoparticles. *Microchim. Acta*. **186**, 386 (2019).
39. Galicia, M., Li, X. & Castaneda, H. Interfacial characterization of single- and multi-walled CNT-Doped Chitosan scaffolds under two flow conditions. *J. Electrochem. Soc.* **161**, H751 (2014).
40. Hussain, S. et al. WS_2/$CoSe_2$ heterostructure: a designed structure as catalysts for enhanced hydrogen evolution performance. *J. Ind. Eng. Chem.* (2018).
41. Wang, K. et al. CoSe2 necklace-like nanowires supported by carbon fiber paper: a 3D integrated electrode for the hydrogen evolution reaction. *J. Mater. Chem. A*. **3**, 9415–9420 (2015).
42. Zhang, Y., Gao, L., Hensen, E. J. M. & Hofmann, J. P. Evaluating the stability of Co_2P electrocatalysts in the hydrogen evolution reaction for both acidic and alkaline electrolytes. *ACS Energy Lett.* **3**, 1360–1365 (2018).
43. Rison, S. et al. Non-enzymatic electrochemical determination of salivary cortisol using ZnO-graphene nanocomposites. *RSC Adv.* **11**, 37877–37885 (2021).
44. Zhang, J., Wang, X., Meng, W., Han, C. & Leng, C. Electrochemical dopamine detection using a Fe/Fe3O4@C composite derived from a metal-organic framework. *ChemistrySelect* **7**, e202201534 (2022).
45. Wei, X. et al. A novel electrochemical sensor based on DUT-67/ZnCo2O4-MWCNTs modified glassy carbon electrode for the simultaneous sensitive detection of dopamine and uric acid. *Colloids Surf. A*. **674**, 131921 (2023).
46. Zhang, L. & Lin, X. Electrochemical behavior of a covalently modified glassy carbon electrode with aspartic acid and its use for voltammetric differentiation of dopamine and ascorbic acid. *Anal. Bioanal. Chem.* **382**, 1669–1677 (2005).

47. Pallavi, K. M., Mamatha, G. P., Nagaraju, G. & Soundarya, T. L. Facile synthesis of NaTaO3 nanoparticles and fabrication of nanostructured NaTaO3 for detection of dopamine. *Inorg. Chem. Commun.* **158**, 111427 (2023).
48. Aldughaylibi, F. S. et al. Development of molybdenum trioxide based modified graphite sheet electrodes for enhancing the electrochemical sensing of dopamine. *Mater. Sci. Semiconduct. Process.* **173**, 108107 (2024).
49. Njagi, J., Chernov, M. M., Leiter, J. C. & Andreescu, S. Amperometric detection of dopamine in vivo with an enzyme based carbon fiber microbiosensor. *Anal. Chem.* **82**, 989–996 (2010).
50. Florescu, M. & David, M. Tyrosinase-based biosensors for selective dopamine detection. *Sensors* **17**, 1314 (2017).
51. S, S., Y, K. & J. S, A. N. & A highly stable copper nano cluster on nitrogen-doped graphene quantum dots for the simultaneous electrochemical sensing of dopamine, serotonin, and nicotine: a possible addiction scrutinizing strategy. *J. Mater. Chem. B.* **10**, 3974–3988 (2022).
52. Hussain, S., Abbas Zaidi, S., Vikraman, D., Kim, H. S. & Jung, J. Facile preparation of tungsten carbide nanoparticles for an efficient oxalic acid sensor via imprinting. *Microchem. J.* **159**, 105404 (2020).
53. Zhong, M., Teng, Y., Pang, S., Yan, L. & Kan, X. Pyrrole–phenylboronic acid: a novel monomer for dopamine recognition and detection based on imprinted electrochemical sensor. *Biosens. Bioelectron.* **64**, 212–218 (2015).
54. Qian, T., Wu, S. & Shen, J. Facilely prepared polypyrrole-reduced graphite oxide core–shell microspheres with high dispersibility for electrochemical detection of dopamine. *Chem. Commun.* **49**, 4610–4612 (2013).
55. Kokulnathan, T., Wang, T. J., Kumar, E. A. & Duraisamy, N. An-Ting, L. An electrochemical platform based on yttrium oxide/boron nitride nanocomposite for the detection of dopamine. *Sens. Actuators B.* **349**, 130787 (2021).
56. Ko, S. H., Kim, S. W. & Lee, Y. J. Flexible sensor with electrophoretic polymerized graphene oxide/PEDOT:PSS composite for voltammetric determination of dopamine concentration. *Sci. Rep.* **11**, 21101 (2021).
57. Ahuja, T., Mir, I. A. & Kumar, D. R. Biomolecular immobilization on conducting polymers for biosensing applications. *Biomaterials* **28**, 791–805 (2007).

Acknowledgements

This project was partly supported by Researchers Supporting Project number (RSP2025R231), King Saud University, Riyadh, Saudi Arabia. The authors K. K and A.A thankfully acknowledge Khalifa University of Science and Technology, Abu Dhabi, United Arab Emirates for their funding support. Author A.S would like to sincerely thank SVCE Management for providing Intramural Faculty Research Funding (Ref. No.: SVCE/IRG/R & D/ACH/2023-2024/04).

Author contributions

A.S.: conceptualization, methodology and writing-original draft preparation C.V.: methodology, and resources A.I.A.: resources and writing-review and editing K.K.: methodology and resources T.M.: methodology and writing- review and editing A.A.: visualization, supervision, validation H-S.K.: conceptualization, visualization, supervision, validation and funding acquisition D.V.: conceptualization, visualization, methodology and writing-original draft preparation.

Declarations

Competing interests

The authors declare no competing interests.

Additional information

Supplementary Information The online version contains supplementary material available at https://doi.org/10.1038/s41598-024-82355-1.

Correspondence and requests for materials should be addressed to D.V. or A.A.